



Application of pole-zero cancellation circuit in nuclear signal filtering and shaping algorithm

Huai-Ping Wang^{1,3} · Jian-Bin Zhou¹ · Xiao-Ping Ouyang² · Xian-Guo Tuo¹ · Xu Hong¹ · Yi Liu¹ · Jie Yu¹ · You-Xian Jin¹

Received: 30 March 2021 / Revised: 29 May 2021 / Accepted: 7 June 2021 / Published online: 14 August 2021

© China Science Publishing & Media Ltd. (Science Press), Shanghai Institute of Applied Physics, the Chinese Academy of Sciences, Chinese Nuclear Society 2021

Abstract In radiation measurement and digital nuclear spectrum systems, traditional nuclear signal processing circuits in nuclear electronics have been gradually replaced by digital algorithm modules with the application of high-performance programmable hardware logic devices (such as FPGA or DSP). Referring to the digital realization method of inverse RC integral circuit systems, the function of the pole-zero cancellation (PZC) circuit was analyzed, a new modified cascade equivalent model of PZC was established, and the time-domain digital PZC (DPZC) recursive algorithm was derived in detail in this study. Two parameters k_1 and k_D are included in the new algorithm, where k_1 should match the exponential decay time constant of the input signal to realize the pole-zero compensation, while the decay time constant of the output signal can be changed with the adjustable parameter k_D (which is larger than the decay time constant of the input signal). Based on the new DPZC algorithm module, two trapezoidal (triangular) shaping filters were designed and implemented. The

amplitude–frequency characteristics of the output signal of the proposed trapezoidal shaping algorithm and the convolution trapezoidal shaping algorithm were compared, with fixed peaking time. The results show that the trapezoidal shaping algorithm based on DPZC can better suppress high-frequency noise. Finally, based on the NaI (TI) scintillator ($\varphi 75 \text{ mm} \times 75 \text{ mm}$) detector and ^{137}Cs source, the effect of the k_D value on the energy resolution of the DPZC trapezoidal (triangular) shaping algorithm was studied. The experimental results show that, with an increase in k_D , the energy resolution of the system improved and reached the maximum when k_D was greater than 10, and the optimal energy resolution of the system was 7.72%.

Keywords Pole-zero cancellation · C–R inverse system · Trapezoidal/ triangular shaping · Amplitude–frequency characteristics · Energy resolution

This work was supported by the National Natural Science Foundation of China (Nos. 11975060, 12005026, and 12075038) and the Fund of Robot Technology Used for Special Environment Key Laboratory of Sichuan Province (No. 19kftk02).

✉ Jian-Bin Zhou
zjb@cdut.edu.cn

¹ College of Nuclear Technology and Automation Engineering, Chengdu University of Technology, No. 1 East 3 Road, Erxian Bridge, Chenghua District, Chengdu 610059, China

² Northwestern Institute of Nuclear Technology, Xi'an 710024, China

³ Engineering Research Center of Nuclear Technology Application (East China University of Technology), Ministry of Education, Nanchang 330013, China

1 Introduction

The digital pulse processing (DPP) method has been widely studied and applied in the area of radiation measurement and nuclear spectrum systems. A typical digital nuclear spectrum system is illustrated in Fig. 1 [1]. The first stage presents a combination of detector and preamplifier, which transforms nuclear energy into electrical signal; in the second stage, the pole-zero cancellation (PZC) circuit is applied to adjust the pulse shape, which is an elimination procedure of the pole in the preamplifier transform function and zero in the PZC circuit; therefore, the PZC circuit eliminates the undershoot in the pulse and implements the pulse width adjustment. The third stage

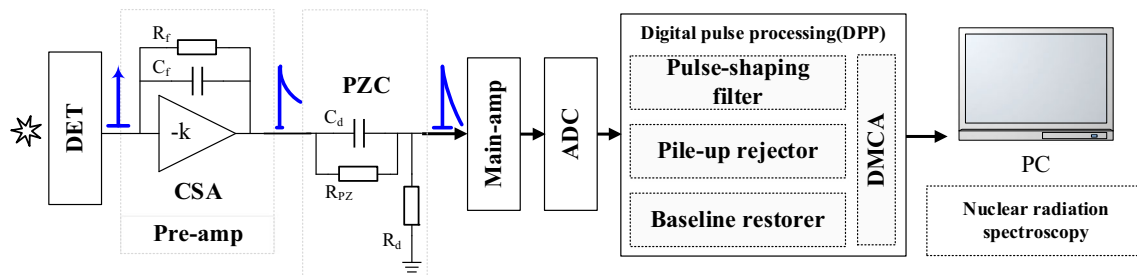


Fig. 1 Typical block diagram of a digital nuclear spectrum system

presents the main amplifier, which adjusts the amplitude of the pulse signal; then, with the high-speed ADC transformation in the fourth stage, the information of the pulse signal data is delivered to DPP to implement processes including digital filter shaping, baseline restoration, pile-up rejection, and multi-channel pulse amplitude analysis. Finally, the data are transferred to a portable computer for spectrometer analysis.

Generally, the output pulse signal of the first stage (detector and RC feedback charge-sensitive amplifier) is an exponential decay voltage pulse signal with a fast-rising edge and a slow-falling edge that finally lands to the baseline [2]. Under the circumstance of a high counting rate, the slow-falling pulse trailing edge increases the probability of pulse pile-up, which results in baseline drifting, and the subsequent amplifier may be blocked. The synthesis of these factors will finally cause drifting of the energy peak channel and degradation of the energy resolution of the nuclear spectrometer [3–6]. In traditional nuclear electronics, analog PZC circuits are often used to narrow the width of the preamplifier output signal, which finally reduces pulse pile-up. However, it is difficult to realize accurate pole-zero compensation exactly; unsuitable compensation processing seriously affects the stability of the baseline and may degrade the energy resolution. With the rapid development of digital signal processing and programmable hardware logic circuits (including FPGA and DSP), it is possible to realize the digitization of signal processing circuit modules in traditional nuclear electronics. Compared with the traditional analog PZC circuit, digital PZC (DPZC) performs better in terms of reliability and flexibility. Geraci et al. designed an automatic pole-zero/pole-zero digital compensator that can be implemented in an FPGA for high-resolution spectroscopy and introduced an equivalent pole-zero couple to accurately compensate for the nuclear pulse signal of the long decay time constant sampled in real time [7]. Zhou et al. established a mathematical model of a PZC circuit using a numerical differential method, which can easily realize the effect of an analog PZC circuit [8]. Saxena and Hawari presented a block diagram of the digital implementation of PZC for RC feedback preamplifier pulses and the transfer

function of the DPZC network in the Z domain. The pulse deconvolution technique was developed to reconstruct the original detector signal from the RC preamplifier, and a real-time high-resolution and high-throughput adaptive DPP system was designed and implemented [9]. These DPZC algorithms are directly derived from the mathematical model of the traditional analog PZC circuit; therefore, the decay time constant of the output pulse signal is generally smaller than that of the input pulse signal. In this study, a modified cascade model of PZC was obtained using an inverse system analysis method, and its digital recursive algorithm was derived. The novel algorithm module can easily adjust the decay time constant of the output pulse signal arbitrarily to be larger or smaller than the original decay time constant of the input pulse signal.

Furthermore, the shaping filter of the nuclear pulse can correct the ballistic deficit, reduce the probability of pulse pile-up, and improve the signal-to-noise ratio (SNR) to optimize the performance of the nuclear spectrometer. Theoretically, the optimal shaping filter for the nuclear pulse signal should be an ideal infinite peaked filter; however, it cannot be realized in a limited time domain. Generally, CR–(RC)ⁿ, trapezoidal (triangular), and cusp-like shaping filters are commonly applied in practical applications. The CR–5(RC)ⁿ shaping filter comprises a simple C–R differential circuit connected in series with a group of *n*-order R–C integral networks, and it can realize the transformation from a negative exponential decay pulse signal to a quasi-Gaussian pulse signal. Owing to their simple circuit structure, CR–(RC)ⁿ shaping filters have been widely used in analog nuclear spectrum systems. Nakhostin designed a digital recursive algorithm by calculating the Z-transform transfer function of a CR–(RC)ⁿ shaping filter within the fourth-order, focusing on the analysis of the noise performance [10]. Liu et al. designed a modified shaping filter algorithm of CR–(RC)^m by replacing the C–R differential circuit with a PZC circuit and deployed the algorithm in FPGA [11]. The trapezoidal (triangular) shaping filter changes a negative exponential decay signal into a trapezoidal (or triangular) pulse output. It has the advantages of a simple algorithm structure, convenient parameter adjustment, short shaping time,

immunity to the ballistic deficit, and easy implementation in programmable hardware logic circuits (such as FPGA or DSP). It has been widely applied to digital nuclear spectrum systems. Jordanov et al. designed a trapezoidal (triangular) shaping algorithm using a digital synthesis method. The algorithm structure is very simple, and the shaping parameters are easily valued. In the programmable hardware logic circuit, only a delay pipeline, adder/subtractor, accumulator, and multiplier are needed [12–14]. Imperiale and Imperiale designed a trapezoidal (triangular) shaping algorithm using the Z-transform method after establishing a trapezoidal (triangular) shaping combination function [15]. Kafae proposed a bipolar cusp-like shaping filter algorithm that can achieve baseline recovery and pile-up correction. The filter adopts a recursive shaping algorithm in the time domain and convolution shaping in the frequency domain. The shaping parameters can be adjusted flexibly and easily implemented in an FPGA or other DPP systems [16]. Liu et al. proposed a cusp-like pulse shaping method based on the recursive formula of the time-domain digital difference and studied in detail the effect of the time constant (τ) on the shaping pulse flat top [17]. These digital filter shaping algorithms for nuclear pulse signals are useful for the design of the DPZC trapezoidal shaping filter algorithm in this study.

Referring to our previous C–R differential inverse system analysis method, the numerical differential and inverse system method was employed to study the digital realization of a traditional PZC circuit. By establishing a new improved PZC equivalent model, we derived the digital recursive algorithm of PZC that can be easily implemented in a programmable hardware logic circuit (such as FPGA or DSP). Then, two types of novel trapezoidal (triangular) shaping algorithms were designed using the DPZC algorithm module through a digital synthesis method, which provides a new idea for the design of shaping algorithms for high-resolution digital nuclear spectrum systems.

2 Digital recursive algorithm of PZC circuit

2.1 Fundamental principle of PZC

The detector converts radiation energy into an impulse signal and outputs a negative exponential decay pulse signal via an RC feedback amplifier. The rising edge of the nuclear pulse signal rises quickly, and the trailing edge falls slowly to the baseline, producing a long tail. The analog PZC circuit is used to process the long minus exponential decay pulse signal in traditional nuclear electronics, as shown in Fig. 1.

The output of the RC feedback amplifier can be expressed using Eq. (1), where $\tau_f = R_f C_f$.

$$v_i(t) = \frac{Q}{C_f} \cdot \exp(-t/\tau_f) \tag{1}$$

Equation (2) can be obtained using the Laplace transform of Eq. (1).

$$V_i(s) = \frac{Q}{C_f} \cdot \frac{1}{s + 1/\tau_f} \tag{2}$$

The Laplace transform equation of the transfer function of the traditional analog PZC circuit shown in Fig. 1 is as follows:

$$H(s) = \frac{V_o(s)}{V_i(s)} = \frac{R_d}{R_d + s \cdot C_d // R_{PZ}} = \frac{s + 1/\tau_1}{s + 1/\tau_2}, \tag{3}$$

where $\tau_1 = R_{PZ} C_d$ and $\tau_2 = (R_d // R_{PZ}) \cdot C_d$.

According to Eqs. (2) and (3), the expression of the output signal of the analog PZC circuit is given by Eq. (4).

$$V_o(s) = V_i(s) \cdot H(s) = \frac{Q}{C_f} \cdot \frac{1}{s + 1/\tau_f} \cdot \frac{s + 1/\tau_1}{s + 1/\tau_2} \tag{4}$$

If $\tau_1 = \tau_f$, then Eq. (4) can be expressed by Eq. (5).

$$V_o(s) = \frac{Q}{C_f} \cdot \frac{1}{s + 1/\tau_2} \tag{5}$$

After the inverse Laplace transform of Eq. (5), the time-domain expression of the output pulse signal can be obtained as follows:

$$v_o(t) = \frac{Q}{C_f} \cdot \exp(-t/\tau_2). \tag{6}$$

When the pole of the transfer function of the preamplifier and the zero of the transfer functions of the analog PZC circuit are canceled, the output signal can be transformed into a short minus exponential decay pulse signal (the time constant is τ_2).

2.2 Digital recursive algorithm for traditional PZC circuit

According to Kirchhoff’s current law, the voltage transfer equation of the analog PZC circuit displayed in Fig. 1 can be established as follows:

$$\frac{V_i(t) - V_o(t)}{R_{PZ}} + C_d \cdot \frac{d(V_i(t) - V_o(t))}{dt} = \frac{V_o(t)}{R_d}. \tag{7}$$

The continuous analog pulse signal can be discretized quickly using a high-speed ADC, and $V_i(t)$ and $V_o(t)$ can be expressed as $x[n]$ and $y[n]$, respectively. Let $k_1 = \Delta t/(R_{PZ} \cdot C_d)$ and $k_2 = \Delta t/(R_d \cdot C_d)$, then the PZC digital recursive equation derived from Eq. (7) is given by:

$$\begin{cases} y[n] = \frac{(1 + k_1) \cdot x[n] - x[n - 1] + y[n - 1]}{1 + k_1 + k_2} & n \geq 1 \\ y[n] = x[n] = 0 & n \leq 0 \end{cases} \tag{8}$$

When processing the digital nuclear pulse signal [Eq. (8)], the algorithm module can completely replace the traditional PZC circuit. To set the values of the parameters k_1 and k_2 , Δt is determined by the sampling rate of the ADC device, and the denominator ($\tau_1 = R_{PZ} \cdot C_d$) of k_1 should match the decay time constant of the output signal of the RC feedback amplifier. According to Eq. (6), the exponential decay time constant of the output pulse signal is $\tau_2 = (R_d/R_{PZ}) \cdot C_d$, and when the resistance value R_{PZ} is much greater than that of R_d , the time constant can be approximately equal to $R_d C_d$. More specifically, the parameter k_1 realizes pole-zero compensation, and k_2 realizes the pulse signal width adjustment (the time constant can only be smaller than the input signal).

By carefully analyzing Eq. (8) and deeply understanding the function of the PZC circuit on the nuclear pulse signal, the traditional PZC circuit can be expressed as an improved cascade equivalent model, as shown in Fig. 2a; thus, the long minus exponential decay pulse signal is first recovered to a step signal by the CR^{INV} system, and then output to a narrow minus exponential decay pulse signal by the CR differential circuit.

Referring to our previous study on the RC inverse system (RC^{INV}), we investigated the CR system and aimed to obtain the digital recursive algorithm of the CR inverse system (CR^{INV}) by analyzing the digital recursive algorithm of the CR system.

The input signal is given by $V_{di}(t)$, and the output signal is $V_{do}(t)$. According to the equation of the CR differential system, which was derived earlier [18]:

$$\frac{dV_{di}(t)}{dt} - \frac{dV_{do}(t)}{dt} = \frac{V_{do}(t)}{R_{d1} \cdot C_{d1}}. \tag{9}$$

Taking a sufficiently small time interval (e.g., $\Delta t = 10$ ns), $V_{di}(t)$ and $V_{do}(t)$ can be digitized into $x[n]$ and $y[n]$, respectively, and Eq. (10) is obtained, where $n = 0, 1, 2, \dots$, $k_D = \Delta t / (R_{d1} C_{d1})$.

$$y[n] = \frac{y[n-1] + x[n] - x[n-1]}{1 + k_D} \tag{10}$$

The inverse system of the C–R differential circuit was defined as CR^{INV} . To distinguish from the above C–R

differential circuit, the resistance and capacitance are expressed as R_I and C_I , respectively, and $k_I = \Delta t / (R_I C_I)$. Using the C–R inverse transformation in Eqs. (10, 11) can be obtained as

$$x[n] - x[n-1] = (1 + k_I) \cdot y[n] - y[n-1]. \tag{11}$$

Rearranging Eq. (11), we obtain Eq. (12).

$$x[n] - x[n-1] = k_I \cdot y[n] + (y[n] - y[n-1]) \tag{12}$$

If the initial values of the input and output signals are zero, Eq. (13) can be obtained using the digital integral transformation of Eq. (12), which is a digital recursive algorithm of the C–R inverse system. Equation (13) can be easily realized using a digital system, and the corresponding block diagram is shown in Fig. 2b.

$$x[n] = k_I \cdot \sum_{i=0}^N y[i] + y[n] \tag{13}$$

Suppose the signal $y[n]$ passes through the C–R inverse system to obtain the output signal $x[n]$, and the signal $x[n]$ passes through the C–R differential system to obtain the signal $z[n]$; the derivation process for the signal transformation can be described as follows.

Using the C–R differential system, the signal $x[n]$ is converted into signal $z[n]$. According to Eq. (10), Eq. (14) can be obtained.

$$z[n] = \frac{z[n-1] + x[n] - x[n-1]}{1 + k_D} \tag{14}$$

The signal $x[n]$ is obtained from the signal $y[n]$ by the C–R inverse system transformation.

Substituting $x[n] = k_I \cdot \sum_{i=0}^n y[i] + y[n]$ into Eq. (14) produces Eq. (15).

$$z[n] = \frac{z[n-1] + k_I \cdot \sum_{i=0}^n y[i] + y[n] - (k_I \cdot \sum_{i=0}^{n-1} y[i-1] + y[n-1])}{1 + k_D} \tag{15}$$

By rearranging Eq. (15), we obtain Eq. (16).

$$z[n] = \frac{z[n-1] + (1 + k_I) \cdot y[n] - y[n-1]}{1 + k_D} \tag{16}$$

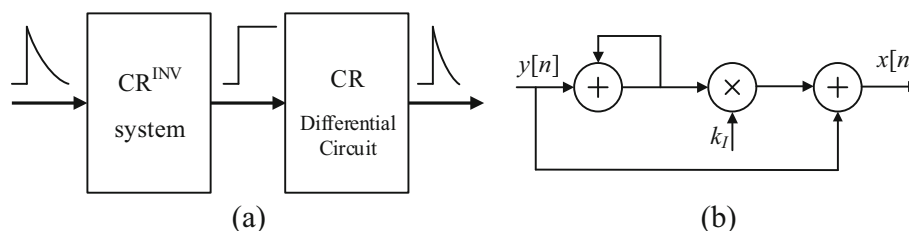


Fig. 2 Improved cascade model of PZC and block diagram of the digital recursive algorithm for CR^{INV} system. **a** Improved cascade equivalent model of PZC circuit. **b** Block diagram of the digital recursive algorithm for CR^{INV} system

Equation (16) is the digital recursive algorithm of the improved cascade equivalent model of the PZC circuit shown in Fig. 2a, which is different from Eq. (8). The reasons for this are as follows.

The C–R part of the PZC circuit displayed in Fig. 1 is equivalent to the result that the capacitor C_d is connected in series to the parallel of resistances R_d and R_{PZ} .

Therefore,

$$k = \frac{\Delta t}{(R_{PZ} // R_d) \cdot C_d} = \frac{\Delta t}{C_d \cdot \frac{R_{PZ} \cdot R_d}{R_{PZ} + R_d}} \tag{17}$$

By organizing Eq. (17), we obtain Eq. (18).

$$k = \frac{\Delta t}{R_{PZ} \cdot C_d} + \frac{\Delta t}{R_d \cdot C_d} \tag{18}$$

In Eq. (8), $k_1 = \Delta t / (R_{PZ} C_d)$, $k_2 = \Delta t / (R_d C_d)$, and $k = k_1 + k_2$. In Eq. (16), $k_I = \Delta t / (R_I C_I)$, $k_D = \Delta t / (R_{d1} C_{d1})$; R_I and R_{PZ} have the same values. R_I and C_I are the parameters of the C–R inverse system shown in Fig. 2a. When the pole-zero compensation condition is satisfied, $k_I = k_1$. Comparing Eq. (8) with Eq. (16), we can see that the numerator part is the same, but the denominator part is different. In Eq. (8), $k = k_1 + k_2 > k_1$, and the decay time constant is inversely proportional to the parameter k ; therefore, it can only achieve a negative exponential signal output with a shorter decay time constant. The value of k_D in Eq. (16) does not have to be constrained by k_1 and k_2 ; that is, the value of k_D can be greater than that of k_1 to achieve a shorter decay time constant minus exponential signal output or less than k_1 to achieve a longer decay time constant minus exponential signal output. Thus, Eq. (16) is more powerful, whereas Eq. (8) is only a specific expression for Eq. (16).

For some purpose, the negative exponential decay pulse signal is sometimes converted into a step signal and sometimes into a narrow pulse signal. In nuclear electronics, the former can be realized using the CR inverse system, whereas the latter requires the use of a PZC circuit. Through analysis of the function of the improved cascade PZC model (i.e., DPZC) represented by Eq. (16), k_I and k_D can be set reasonably to realize an arbitrary adjustment of the decay time constant of the output pulse signal (shorter or longer than the decay time constant of the input pulse signal). Thus, DPZC can realize two functions: the CR^{INV} system and PZC circuit.

MATLAB/Simulink is a software package that is widely used in dynamic system modeling, simulation, and analysis. It provides numerous continuous and discrete signal processing blocks for nuclear pulse signal height analysis and processing. Therefore, it can be used to simulate and analyze nuclear pulse signals and process nuclear spectrum data offline. With the single exponential decay pulse signal

($V_i(t) = V_m \cdot \exp(-t/\tau)$, $V_m = 400$, $\tau = 200$) as excitation, the simulation test expressed in Eq. (16) represents the input–output response of the DPZC model. As shown in Fig. 3 the blue line is the excitation signal, k_I needs to match the decay time constant of the input signal ($k_I = \Delta t / \tau$), and the value of k_D determines the decay time constant of the output signal. When the value of k_D is greater than that of k_I , a shorter decay time constant pulse signal (narrow pulse) is output (green line). When the value of k_D is less than k_I , a longer decay time constant pulse signal (wide pulse) is output (red line). When the value of k_D is zero, the output is a step signal (black line).

3 Design and implementation of digital PZC (DPZC) trapezoidal (triangular) shaping filter algorithm

In the digital nuclear spectrum system, the shaping of the nuclear pulse signal can correct the ballistic deficit, improve the SNR, and reduce the probability of pulse pile-up to improve the resolution. The trapezoidal (triangular) shaping algorithm transforms the input minus exponential decay pulse signal into a trapezoidal (or triangular) pulse output, and the ballistic deficit is naturally immune. It has the advantages of a simple structure, convenient parameter value, short shaping time, and easy realization in a programmable hardware logic circuit (such as FPGA or DSP). Referring to the design idea of the digital synthesis trapezoidal (triangular) shaping algorithm of Jordanov and Knoll [12], two novel trapezoidal (triangular) shaping algorithms can be designed using the DPZC digital

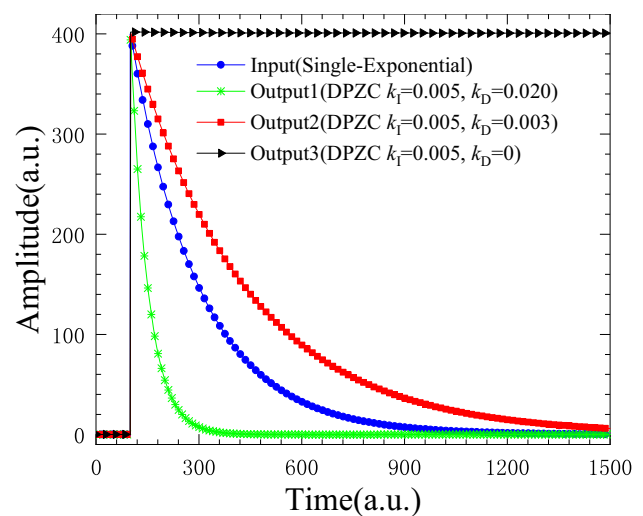


Fig. 3 (Color online) MATLAB simulation results of output response of the DPZC model represented by Eq. (16) when the excitation is a single exponential decay pulse signal

recursive algorithm module represented by Eq. (16). The detailed design is as follows.

The single exponential decay pulse signal ($v_i(t) = V_m \cdot \exp(-t/\tau)$) is digitized into a single exponential decay pulse sequence $v_i[n]$ after sampling using a high-speed ADC. Then, the DPZC digital algorithm module is used to process the discrete sequence $v_i[n]$. The parameters k_I and k_D can be set reasonably, and two new trapezoidal (triangular) shaping algorithms can be designed. A logic diagram of Simulink is shown in Fig. 4.

Algorithm 1: DPZC quasi-impulse response trapezoidal (triangular) shaping algorithm.

If k_D is much larger than k_I , the DPZC algorithm module converts the input pulse signal $v_i[n]$ into a negative exponential pulse signal with a very short decay time constant (quasi-impulse). A logic diagram of Algorithm 1 is shown in Fig. 4a. The input pulse signal $v_i[n]$ is first transformed into a narrow pulse by the DPZC algorithm module, then goes through two stages of delay subtraction unit, and finally provides two accumulation (digital integration) modules.

The recursive equations of Algorithm 1 are as follows:

$$z[n] = \frac{z[n - 1] + (1 + k_I) \cdot y[n] - y[n - 1]}{1 + k_D}, \tag{19}$$

$$d_{k,l}[n] = z[n] - z[n - k] - z[n - l] + z[n - k - l], \tag{20}$$

$$p[n] = p[n - 1] + d_{k,l}[n], \tag{21}$$

$$v_o[n] = v_o[n - 1] + p[n]. \tag{22}$$

Equation (19) is the DPZC digital recursive algorithm module, which needs to match the input pulse signal $v_i(-t)$ decay time constant, and k_D is much larger than k_I , so that the output signal is a narrow pulse (quasi-impulse). Equation (20) is a two-stage delay subtraction module. The parameter k is the width of the trapezoid (triangle) hypotenuse, and l is the width of the sum of the trapezoid flat top and k . When l is equal to k , Algorithm 1 is trapezoidal shaping. In addition, the value of $(l + k)$ should be less than the pulse width of the input signal. Meanwhile, Eqs. (21) and (22) are accumulation (digital integration) modules.

Algorithm 2: DPZC step-response trapezoidal (triangular) shaping algorithm.

If k_D is zero, the DPZC algorithm module transforms the input pulse signal $v_i[n]$ into a step signal. A logic diagram of Algorithm 2 is presented in Fig. 4b. First, the input pulse $v_i[n]$ is transformed into a step signal by the DPZC algorithm module, and then the trapezoidal (triangular) shaping can be realized by a two-stage delay subtraction unit and one-stage accumulation (digital integration) unit.

Algorithm 2 requires only Eqs. (19)–(21) in Algorithm 1; hence, the algorithm structure is simpler. The value of k_D is zero, whereas the other parameters have the same value as Algorithm 1.

The above two shaping algorithms have simple structures, clear parameter meanings, convenient value

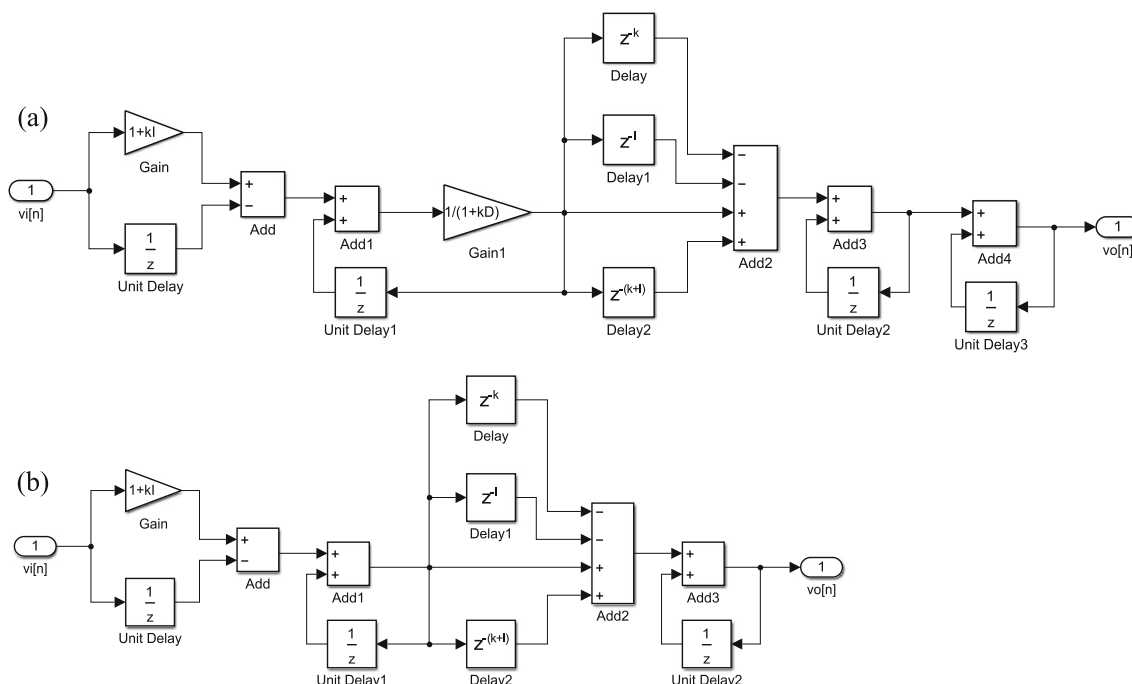


Fig. 4 Logic diagram of the DPZC trapezoidal/triangular shaper in Simulink. a Logic diagram of DPZC quasi-impulse response trapezoidal (triangular) shaping algorithm. b Logic diagram of DPZC step-response trapezoidal (Triangular) shaping algorithm

selection, and easy implementation in programmable hardware logic circuits such as FPGA or DSP.

The simulation of the DPZC trapezoidal (triangular) shaping filter algorithm is shown in Fig. 5. The blue line represents the input single exponential decay pulse signal ($v_i[n] = V_m \cdot \exp(-n \cdot T_s / \tau)$, $V_m = 1$, $T_s = 0.05 \mu s$, $\tau = 5 \mu s$). Figure 5a shows the simulation results of DPZC shaping filter Algorithm 1, where k_I is 0.01, the input pulse signal $v_i[n]$ matches the decay time constant, k_D is 1, and the black line is the DPZC algorithm module output: a narrow pulse signal (quasi-impulse). The magenta line is a trapezoidal-shaped output pulse of Algorithm 1 ($k = 100$, $l = 120$). The green line is a triangular-shaped output pulse of Algorithm 1 (k and l are 100). Figure 5b shows the simulation result of DPZC shaping filter Algorithm 2, where the value of k_D is zero, and the other parameters are the same as those in Fig. 5a. The black line is the DPZC algorithm module output step signal, the magenta line is the Algorithm 2 output trapezoidal shaping pulse, and the green line is the Algorithm 2 output triangular shaping pulse.

4 Experiment and performance

Generally, the performance of a shaping filter algorithm can be evaluated from many aspects, such as correcting ballistic deficit, improving the SNR, executing algorithm time, and improving resolution [19]. The trapezoidal (triangular) shaping algorithm is naturally immune to ballistic deficits. The main performance of the DPZC trapezoidal (triangular) shaping algorithm is analyzed regarding two aspects: amplitude–frequency characteristics and improving resolution.

4.1 Amplitude–frequency characteristic

For the DPZC quasi-impulse response trapezoidal (triangular) shaping algorithm model shown in Fig. 4a, the Z-transform equation of the shaping filter transfer function can be derived from Eqs. (19)–(22), as follows:

$$H(z) = H_1(z) \cdot H_2(z) \cdot H_3(z) \cdot H_4(z) = \left(\frac{1 + k_I - z^{-1}}{1 + k_D - z^{-1}} \right) \cdot \frac{(1 - z^{-k} - z^{-l} + z^{-k-l})}{k^2} \cdot \left(\frac{1}{1 - z^{-1}} \right)^2 \tag{23}$$

Equation (23) constitutes four subsystems, whose transfer function Z-transform equations are:

$$H_1(z) = \frac{1 + k_I - z^{-1}}{1 + k_D - z^{-1}}, \text{ DPZC algorithm module;}$$

$$H_2(z) = \frac{1 - z^{-k} - z^{-l} + z^{-k-l}}{k^2}, \text{ where the numerator is the DS, and the denominator is the scale factor;}$$

$$H_3(z) = H_4(z) = \frac{1}{1 - z^{-1}}, \text{ all of which are digital integrators.}$$

Taking the same shaping parameters, the amplitude–frequency characteristic curve of the DPZC quasi-impulse response trapezoidal (triangular) shaping algorithm module can be drawn according to Eq. (23), as shown by the red curve (B) in Fig. 6a, while the blue curve (A) in Fig. 6a represents the amplitude–frequency characteristic curve of the trapezoidal (triangle) shaping filter algorithm model designed by Jordanov [11], and the purple curve (C) in Fig. 6a is the difference between curves (A) and (B). The two shaping filter algorithm modules exhibit the same performance in the passband, but curve (B) is slightly better than curve (A) in the stopband for high-frequency noise suppression. More specifically, the DPZC quasi-impulse response trapezoidal (triangular) algorithm module

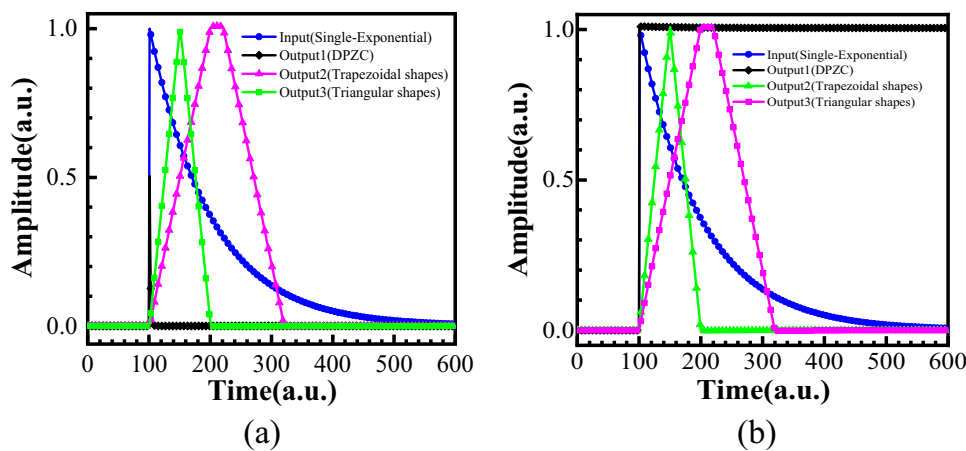


Fig. 5 (Color online) Simulation of DPZC trapezoidal (triangular) shaping filter algorithm. $v_i[n] = \exp(-n \cdot T_s / \tau)$, $T_s = 0.05 \mu s$ (ADC sampling rate: 20 MSPS), $\tau = 5 \mu s$. **a** DPZC quasi-impulse response trapezoidal (triangular) shaper. Shaping parameters: $k_I = 0.01$,

$k_D = 1$; trapezoidal shaping $k = 100$, $l = 120$; triangular shaping $k = 100$, $l = 100$. **b** DPZC step-response trapezoidal shaper. Shaping parameters: $k_I = 0.01$, $k_D = 0$; trapezoidal shaping $k = 100$, $l = 120$; triangular shaping $k = 100$, $l = 100$

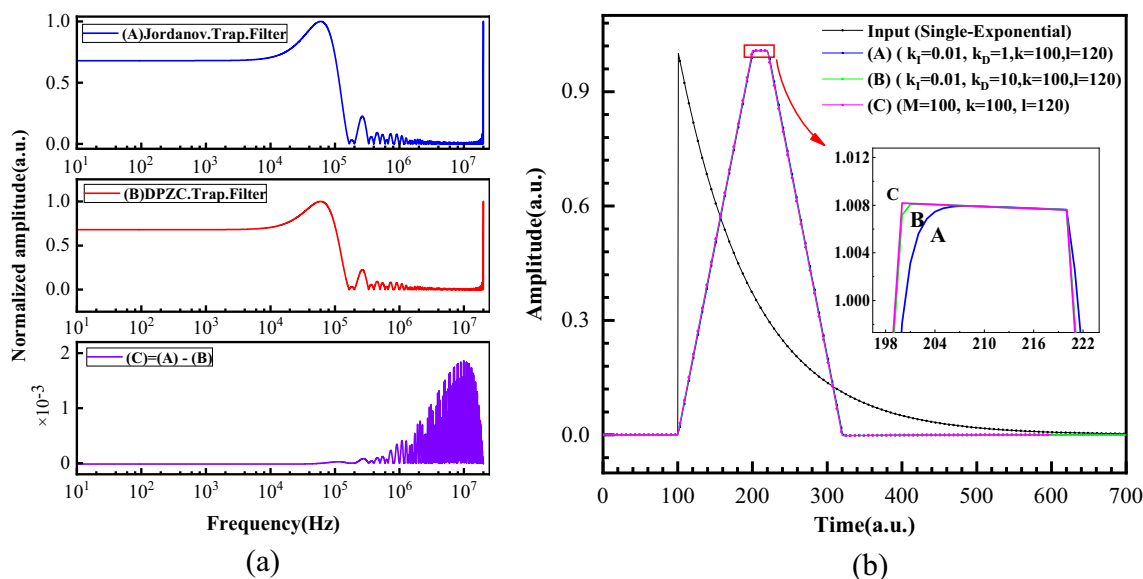


Fig. 6 (Color online) Comparison of amplitude–frequency characteristics of two shaping filters and analysis of shaping difference. **a** Comparison of amplitude–frequency characteristics of the digital synthesis trapezoidal shaper (Jordanov) and DPZC quasi-impulse response trapezoidal shaper. Shaping parameters: $M = \exp(-k_I)$,

exhibits better performance in high-frequency noise suppression for the same shaping parameters.

The reason for the difference in the amplitude–frequency characteristics between the two trapezoidal (triangular) shaping algorithm modules is explained through the simulation experiment of single exponential decay pulse signal shaping.

A single exponential decay pulse signal ($v_i(t) = \exp(-t/\tau)$, $\tau = 100$) was used as the excitation. The trapezoidal shaping parameters were $k = 100$ and 120 . The simulation output of the algorithm module is shown in Fig. 6b. Curves A (blue line) and B (green line) are the outputs of the DPZC quasi-impulse response trapezoidal shaping filter algorithm, k_I is 0.01, k_D of curve A is 1, and k_D of curve B is 10. Curve C (the magenta line) is the output of Jordanov’s trapezoidal shaping algorithm, and M is 100. Figure 6b shows that the upper corners of the leading edges of curves A and B rise exponentially to the flat top. The smaller the k_D value, the longer the transition zone. Meanwhile, the leading edge of curve C increases linearly to the flat top. Owing to the exponentially rising transition zone in the upper corner to the flat top of the output signal of the DPZC quasi-impulse response shaping algorithm module, there is a difference in the high-frequency noise suppression performance of the stopband of the amplitude–frequency characteristics of the two trapezoidal shaping algorithms.

$k_I = 0.01$, $k_D = 10$, $k = 100$, $l = 120$. **b** Analysis of shaping difference. Curve A is DPZC quasi-impulse response trapezoidal shaping, $k_D = 1$. Curve B is DPZC quasi-impulse response trapezoidal shaping, $k_D = 10$. Curve C is Jordanov’s trapezoidal shaping, $M = 100$

4.2 Energy spectrum measurement

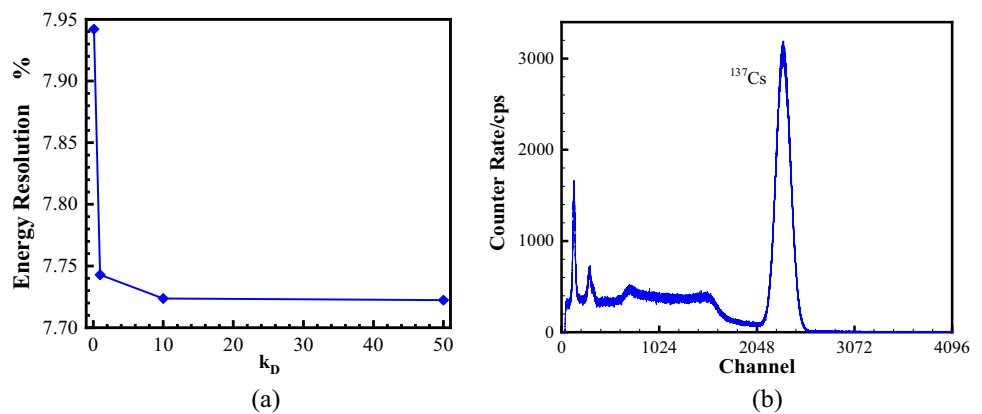
In the experiment, a $\varnothing 75$ mm \times 75 mm NaI (Tl) scintillator detector was employed to measure the radiation of the ^{137}Cs source. The nuclear pulse signal from the preamplifier was directly sampled and converted into a digital pulse signal using a high-speed ADC (AD9235, 12-bit, sampling rate of 20 MSPS), and the nuclear pulse data were analyzed offline using the nuclear energy spectrum.

The above analysis shows that when the shaping parameters are determined, the shaping effect of the DPZC quasi-impulse response trapezoidal (triangular) shaping algorithm module is related to the value of parameter k_D , which seriously affects the high-frequency noise suppression performance of the shaping filter, thus affecting the change in energy resolution. For the offline spectrum analysis of the ^{137}Cs pulse data above, the shaping algorithm used the DPZC quasi-impulse response trapezoidal (triangular) shaping algorithm, and the shaping parameters k and l were 30 and 35, respectively, k_I was set to match the input signal decay time constant (approximately 320 ns), and k_D was set to different values for the energy spectrum analysis. The relationship between k_D and the energy resolution is shown in Fig. 7a. When k_D was 0.1, the energy resolution was 7.94%. As k_D increased gradually, the energy resolution decreased. When k_D was 10, the energy resolution was 7.72%; and, although k_D increased, the energy resolution remained unchanged.

Fig. 7 Effect of k_D on energy resolution and the experimental gamma spectrum.

$\varphi 75 \text{ mm} \times 75 \text{ mm NaI (Tl)}$ @ ^{137}Cs 0.662 MeV.

a Relationship between k_D and energy resolution. **b** Gamma spectrum obtained using the DPZC quasi-impulse response trapezoidal shaping algorithm



Experimental platform: DET: $\varphi 75 \text{ mm} \times 75 \text{ mm NaI}$ (Tl) scintillation detector; source: ^{137}Cs ; shaping parameters: $k = 30$, $l = 35$, $k_D = 10$; measured energy resolution: 7.72% @ ^{137}Cs 0.662 MeV.

The DPZC quasi-impulse response trapezoidal shaping algorithm was used in the DPP module [20]. When k_D was 10, k was 30, l was 35, and the energy spectrum measurement results were obtained after offline processing of the experimental data, as shown in Fig. 7b.

5 Conclusion

By carefully analyzing the function of the PZC circuit in traditional nuclear electronics, the modified cascade equivalent model of the PZC circuit was reestablished. First, the input single exponential decay pulse signal was transformed into a step signal with a CR^{INV} system, and then the step signal was transformed into a negative exponential decay pulse signal with a variable decay constant with a C–R differential circuit. The digital recursive algorithm of the improved cascade equivalent model (DPZC) was derived in detail using digital differential and inverse system methods. In the algorithm, k_I should match the decay time constant of the input signal, and k_D can adjust the pulse width. When k_D is greater than k_I , the pulse width of the signal can be narrowed, and the pulse width of the signal can be widened when k_D is set to less than k_I .

Referring to the digital synthesis idea of the filter shaping algorithm, a trapezoidal (triangular) shaping algorithm was designed and implemented using the DPZC algorithm module. Two filter shaping algorithms, specifically, the DPZC quasi-impulse response trapezoidal (triangular) shaping algorithm and the DPZC step-response trapezoidal (triangular) shaping algorithm, were obtained. Moreover, the algorithms have a simple structure, convenient parameter adjustment, and easy implementation in programmable hardware logic circuits (such as FPGA or DSP). By analyzing the amplitude–frequency

characteristics of the DPZC trapezoidal (triangular) shaping algorithm module, when the shaping parameters are the same, the passband performance of the DPZC trapezoidal (triangular) shaping algorithm module is the same as that of Jordanov's trapezoidal (triangular) shaping algorithm module, but it has a slight advantage in high-frequency noise suppression.

Finally, the offline data of ^{137}Cs were measured using a $\varphi 75 \text{ mm} \times 75 \text{ mm NaI}$ (Tl) scintillation detector and processed using the DPZC trapezoidal (triangular) shaping algorithm module. Furthermore, from the result of the energy spectrum analysis, the relationship curve between k_D and the energy resolution was obtained. When k_D increases from 0.1, the energy resolution decreases from 7.94%; when k_D is 10, the energy resolution is 7.72%, and the increase in k_D has a slight effect on the energy resolution. Since the DPZC trapezoidal shaping algorithm is aimed at the negative exponential decay pulse signal, it can be widely applied in DPP (such as pulse signals originating from a LaBr_3 or HPGe detector).

Author contributions All authors contributed to the study conception and design. Material preparation, data collection, and analysis were performed by Huai-Ping Wang, Jian-Bin Zhou, Xiao-Ping Ouyang, Xian-Guo Tuo, and Xu Hong. The first draft of the manuscript was written by Huaiping Wang and all authors commented on previous versions of the manuscript. All authors read and approved the final manuscript.

References

1. A. Regadío, S. Sánchez-Prieto, M. Prieto et al., Implementation of a real-time adaptive digital shaping for nuclear spectroscopy. *Nucl. Instrum. Methods Phys. Res. A* **735**, 297–303 (2014). <https://doi.org/10.1016/j.nima.2013.09.063>
2. G.F. Knoll, *Radiation Detection and Measurement*, 4th edn. (Wiley, New York, 2012)
3. Y. Liu, M. Wang, W.J. Wan et al., Counting-loss correction method based on dual-exponential impulse shaping. *Synchrotron*.

- Rad. **27**, 1609–1613 (2020). <https://doi.org/10.1107/S1600577520010954>
4. M. Sanchez-Raya, J.A. Gomez-Galan, E. Cojocarú et al., Linear tunable analog front-end electronics for silicon charged-particle detectors. *IEEE Trans. Instrum. Meas.* **64**(2), 418–426 (2015). <https://doi.org/10.1109/tim.2014.2345920>
 5. X. Hong, H.P. Wang, J.B. Zhou et al., Peak tailing cancellation techniques for digital CR–(RC)ⁿ filter. *Appl. Radiat. Isotopes.* **167**, 109471 (2020). <https://doi.org/10.1016/j.apradiso.2020.109471>
 6. M. Nakhostin, M.P. Taggart, P.J. Sellin, A digital pulse shortening method for the mitigation of pulse pile-up effect in scintillation radiation detectors. *J. Instrum.* **14**(4), P04012 (2019). <https://doi.org/10.1088/1748-0221/14/04/P04012>
 7. A. Geraci, A. Pullia, G. Ripamonti, Automatic pole-zero/zero-pole digital compensator for high-resolution spectroscopy: design and experiments. *IEEE Trans. Nucl. Sci.* **46**(4), 817–821 (1999). <https://doi.org/10.1109/nssmic.1998.774313>
 8. J.B. Zhou, X. Hong, R.B. Wang et al., Study of recursive model for pole-zero cancellation circuit. *Nucl. Sci. Tech.* **25**(1), 010403 (2014). <https://doi.org/10.13538/j.1001-8042/nst.25.010403> (in Chinese)
 9. S. Saxena, A.I. Hawari, Digital pulse deconvolution with adaptive shaping for real-time high-resolution high-throughput gamma spectroscopy. *Nucl. Instrum. Methods Phys. Res. A* **954**, 161288 (2018). <https://doi.org/10.1016/j.nima.2018.09.123>
 10. M. Nakhostin, Recursive algorithms for real-time digital CR–(RC)ⁿ pulse shaping. *IEEE Trans. Nucl. Sci.* **58**(5), 2378–2381 (2011). <https://doi.org/10.1109/tns.2011.2164556>
 11. Y.Y. Liu, J.L. Zhang, L.F. Liu et al., Implementation of real-time digital CR–RC^m shaping filter on FPGA for gamma-ray spectroscopy. *Nucl. Instrum. Methods Phys. Res. A* **906**, 1–9 (2018). <https://doi.org/10.1016/j.nima.2018.05.020>
 12. V.T. Jordanov, G.F. Knoll, Digital synthesis of pulse shapes in real time for high resolution radiation spectroscopy. *Nucl. Instrum. Methods Phys. Res. A* **345**, 337–345 (1994). [https://doi.org/10.1016/0168-9002\(94\)91011-1](https://doi.org/10.1016/0168-9002(94)91011-1)
 13. V.T. Jordanov, Unfolding-synthesis technique for digital pulse processing. Part 1: unfolding. *Nucl. Instrum. Methods Phys. Res. Sect. A* **805**, 63–71 (2016). <https://doi.org/10.1016/j.nima.2015.07.040>
 14. V.T. Jordanov, G.F. Knoll, A.C. Huber et al., Digital techniques for real-time pulse shaping in radiation measurements. *Nucl. Instrum. Methods Phys. Res.* **353**(1–3), 261–264 (1994). [https://doi.org/10.1016/0168-9002\(94\)91652-7](https://doi.org/10.1016/0168-9002(94)91652-7)
 15. C. Imperiale, A. Imperiale, On nuclear spectrometry pulses digital shaping and processing. *Measurement* **30**, 49–73 (2001). [https://doi.org/10.1016/s0263-2241\(00\)00057-9](https://doi.org/10.1016/s0263-2241(00)00057-9)
 16. M. Kafaei, A. Moussavi-Zarandi, Baseline restoration and pile-up correction based on bipolar cusp-like shaping for high-resolution radiation spectroscopy. *J.-Korean Phys. Soc.* **68**(8), 960–964 (2016). <https://doi.org/10.3938/jkps.68.960>
 17. J. Liu, J. Yang, G.Q. Zeng et al., Implementation of a cusp-like for real-time digital pulse shaper in nuclear spectrometry. *Nucl. Sci. Tech.* **28**, 103 (2017). <https://doi.org/10.1007/s41365-017-0248-1>
 18. M. Wang, X. Hong, J.B. Zhou et al., Rising time restoration for nuclear pulse using a mathematic model. *Appl. Radiat. Isotopes* **137**, 280–284 (2018). <https://doi.org/10.1016/j.apradiso.2018.01.018>
 19. C.Y. Zhao, H. Xiong, Y.Y. Liu et al., A new digital filter based on sinusoidal function for gamma spectroscopy. *Nucl. Instrum. Methods Phys. Res. A* **944**, 162582 (2019). <https://doi.org/10.1016/j.nima.2019.162582>
 20. G. Gerardi, L. Abbene, A digital approach for real time high-rate high-resolution radiation measurements. *Nucl. Instrum. Methods Phys. Res. A* **768**, 46–54 (2014). <https://doi.org/10.1016/j.nima.2014.09.047>